Scientific Reports

https://doi.org/10.1038/s41598-026-42057-2

Article in Press

Research on the atomic clock signal denoising method based on the hyperbolic tangent smooth threshold function

Received: 18 November 2025

Accepted: 24 February 2026

Published online: 20 March 2026

Cite this article as: Liu Q., Ning X., Hu D. *et al.* Research on the atomic clock signal denoising method based on the hyperbolic tangent smooth threshold function. *Sci Rep* (2026). https://doi.org/10.1038/s41598-026-42057-2

Qiang Liu, Xueyou Ning, Denghua Hu, Liming Wang & Zhentao Wang

Research on the atomic clock signal denoising method based on the hyperbolic tangent smooth threshold function

Qiang Liu[1], Xueyou Ning[1], Denghua Hu[1]✉, Liming Wang[2] & Zhentao Wang[1]

Abstract To address the discontinuity and constant bias issues in traditional hard and soft threshold functions for atomic clock signal denoising, this study proposes a denoising method based on hyperbolic tangent smoothing threshold functions. The approach employs empirical mode decomposition (EMD) to adaptively decompose nonstationary atomic clock signals into a series of intrinsic mode functions (IMFs) and residual components. For each IMF, an improved hyperbolic tangent-based threshold function is constructed, which regulates the transition between hard and soft threshold characteristics through a smoothing factor. The optimal thresholds for each IMF are then determined by Stein's unbiased risk estimate (SURE) criterion combined with a right offset strategy. The denoised IMFs and residual are reconstructed to obtain the final denoised signal. The case study analyses demonstrated that, in comparison with traditional wavelet threshold denoising methods, the proposed method suppressed noise effectively while preserving the smoothness and detailed features of the signal more favorably. Specifically, in terms of noise suppression, the improved thresholding method increased the SNR by 14%, 5% and 26% for cesium clock, hydrogen clock and measured rubidium clock data. In terms of signal fidelity, its RMSE was reduced by 28%, 10% and 25% relative to the soft thresholding method. This method retained the authentic information of the signal while suppressing noise, and exhibited good repeatability. It effectively improved the frequency stability of the time scale, thereby providing a novel technical approach for enhancing the quality of atomic clock data and the frequency stability of the time scale.

Keywords signal processing, wavelet thresholds denoising, empirical mode decomposition, Stein's unbiased risk estimate, adaptive threshold selection

Time, as a fundamental physical quantity that describes the order of material movement and event occurrence, serves as the core foundation of the modern science and technology system. In time-frequency systems, as a precise time generation and holding device, the stability of an atomic clock's output signal directly determines the performance of the time scale. However, atomic clock signals are affected by internal physical mechanisms and external environmental interference, which introduce complex noise and hinder the improvement of time scale accuracy[1,2]. The wavelet threshold denoising method enables visualized analysis in both the time domain and frequency domain simultaneously and can effectively distinguish between target signals and noise, thus becoming one of an important technique for atomic clock signal denoising[3-6]. Nevertheless, traditional hard and soft threshold functions respectively suffer from the Gibbs phenomenon caused by discontinuity at the threshold point, and the problem of excessive signal smoothing due to constant bias. As a result, it is difficult to achieve an effective balance between noise suppression and detail preservation[7].

To address the aforementioned issues, scholars have successively proposed various improved schemes. Qu[8] constructed a continuously

differentiable threshold function and combined it with the SURE criterion for adaptive threshold selection. However, the function form is complex, and the differences in wavelet coefficients across different decomposition scales are not fully considered. Meng[9] proposed a semisoft threshold function, which retains and shrinks wavelet coefficients by adjusting parameters to achieve a smooth transition in the threshold neighborhood. However, this method requires manual parameter setting and cannot be adjusted adaptively. Tao[10] selected multiple indicators, used information entropy to determine their weights, and constructed a comprehensive evaluation index to identify the optimal scale, overcoming the inaccuracy of

[1]Air and Missile Defense College, Air Force Engineering University, Xi'an 710051, China. [2]The 92330 Unit, the Chinese People's Liberation Army, Qingdao 266000, China. email: hudenghua@qq.com

judgment on the basis of a single indicator. However, it requires knowledge of the real signal, which limits its practical application. Wu[11] constructed a parameterized variable threshold function that adaptively adjusts the function form according to the signal energy distribution, which exhibited excellent performance in preserving signal singularity. However, its parameter selection still relies on empirical settings and lacks a global adaptive mechanism. Liu[12] improved the SURE method for short-signal denoising and used a particle swarm optimization algorithm to synchronously optimize the scale factor of the threshold function, enhancing denoising stability for small samples. However, the algorithm has low computational efficiency and fails to fully solve the problem of local optimal solutions.

Overall, existing studies have proposed various improved schemes, but problems such as complex function forms, low computational efficiency, and reliance on the empirical selection of thresholds and parameters still persist. EMD decomposition is a data-driven adaptive decomposition method. It decomposes the signal without requiring predefined basis functions. It is well-suited for processing non-stationary atomic clock signals, offering low reconstruction error and high computational efficiency. While EMD suffers from modal overlap limitations, its variants require manual parameter tuning, involve substantial computational effort, and lack adaptability. Therefore, this paper proposes a method combining "EMD decomposition + improved threshold function + adaptive parameter selection mechanism". It perform wavelet threshold denoising on all IMF components, followed by signal reconstruction based on the denoised results. The improved method effectively suppresses noise while better preserving useful signal information, offering a new technical approach to enhance atomic clock data quality and temporal stability. Case studies were conducted using simulated and measured atomic clock data to validate the algorithm's performance. The structural framework of the paper is shown in Fig. 1.

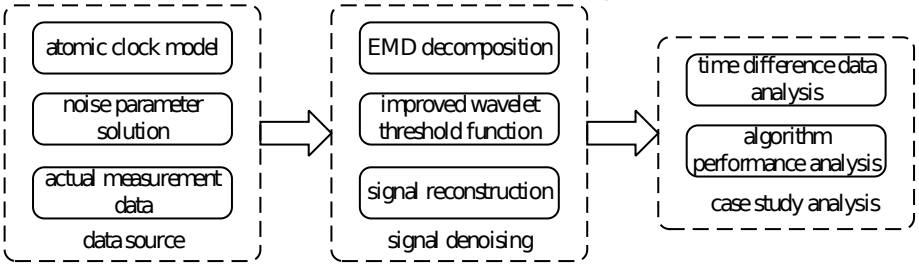

Fig. 1 Structural diagram

Modle and methods

Atomic clock model

As a frequency standard, the cesium atomic clock exhibits excellent long-term frequency stability. Its linear frequency drift caused by aging is

extremely low and can be neglected in practical applications, thus ensuring a relatively small frequency offset. The deviation between its output signal and the ideal reference signal can be systematically decomposed into three core parameters: phase deviation, frequency deviation, and frequency drift. These three parameters form a complete dynamic system that can capture the main noise characteristics and deterministic trends of the cesium clock. Therefore, employing a three-state time series model to describe its evolution is the most classical and effective approach.

On the basis of the aforementioned physical mechanism, the following discrete-time state-space model is established to characterize the properties of the cesium clock. This model defines three key state variables: p_t denotes the clock offset at time t, i.e., the accumulated phase deviation; f_t denotes the frequency deviation at time t; and d_t denotes the frequency drift at time t. Let the time interval be τ; then the state evolution equation of model[13] is as follows:

$$\begin{cases} p_t = p_{t-\tau} + f_{t-\tau}\tau + 1/2 d_{t-\tau}\tau^2 + e \\ f_t = f_{t-\tau} + d_{t-\tau}\tau + m \\ d_t = d_{t-\tau} + s \end{cases} \quad (1)$$

Where e, m, and s are phase deviation, frequency deviation and random noise during frequency drift. p_t is obtained by integrating $f_{t-\tau}$ from the previous moment and is affected by $d_{t-\tau}$ from the previous moment. f_t is derived from integrating $d_{t-\tau}$ from the previous moment, whereas the frequency drift itself is a random walk process. The entire process noise influences the random changes in the system state, accurately describing the long-term instability and random fluctuations of the cesium clock.

Noise parameter solving

The output deviation of an atomic clock is a complex random process composed of the superposition of multiple uncorrelated noise types. To simulate atomic clock data accurately, it is necessary to identify the main noise types and their parameters. These parameters can be obtained by analyzing the Allan variance, a typical indicator of atomic clock frequency stability. There is a clear functional relationship between the variation law of the Allan variance over different averaging times τ and specific noise types. Therefore, the intensity coefficients of various noises can be separated and solved by fitting the measured Allan variance curve.

The overall frequency stability of an atomic clock is composed of four main noise components: white phase modulation (WPM), white frequency modulation (WFM), flicker frequency modulation (FFM), and random walk frequency modulation (RWFM)[14,15]. These noises are uncorrelated with each other, and the total Allan variance can be expressed as the sum of the variances of each noise term.

$$\sigma_y^2(\tau) = \sigma_{y,WP}^2(\tau) + \sigma_{y,WF}^2(\tau) + \sigma_{y,FF}^2(\tau) + \sigma_{y,RW}^2(\tau) \quad (2)$$

The functional relationships between each noise term and the Allan standard deviation are as follows:

$$\begin{cases} \sigma_{y,WP}(\tau) = A_{WP}\sqrt{f_h/\tau^2} \\ \sigma_{y,WF}(\tau) = A_{WF}\sqrt{1/\tau} \\ \sigma_{y,FF}(\tau) = A_{FF} \\ \sigma_{y,RW}(\tau) = A_{RW}\sqrt{\tau} \end{cases} \quad (3)$$

where A_{WP} is the Allan standard deviation of the WPM at $t=1s$ and $f_h=1Hz$; A_{WF}, A_{FF} and A_{RW} are the Allan standard deviations of the WFM, FFM, and RWFM at $t=1s$.

To solve these four noise parameters, it is necessary to measure the Allan standard deviation $s_{y,m}(t_i)$ at multiple averaging times $t_i(i=1,2,\mathrm{L},N)$ and establish the following system of equations:

$$\begin{cases} s_{y,m}(t_1)=A_{WP}\sqrt{f_h/t_1^2}+A_{WF}\sqrt{1/t_1}+A_{FF}+A_{RW}\sqrt{t_1} \\ s_{y,m}(t_2)=A_{WP}\sqrt{f_h/t_2^2}+A_{WF}\sqrt{1/t_2}+A_{FF}+A_{RW}\sqrt{t_2} \\ \mathrm{M} \\ s_{y,m}(t_N)=A_{WP}\sqrt{f_h/t_N^2}+A_{WF}\sqrt{1/t_N}+A_{FF}+A_{RW}\sqrt{t_N} \end{cases} \tag{4}$$

It can be expressed in matrix form as follows:

$$\mathbf{M}\times\mathbf{A}=\mathbf{\Sigma} \tag{5}$$

where

$$\mathbf{M}=\begin{bmatrix} \sqrt{f_h/t_1^2} & \sqrt{1/t_1} & 1 & \sqrt{t_1} \\ \sqrt{f_h/t_2^2} & \sqrt{1/t_2} & 1 & \sqrt{t_2} \\ \mathrm{M} & \mathrm{M} & \mathrm{M} & \mathrm{M} \\ \sqrt{f_h/t_N^2} & \sqrt{1/t_N} & 1 & \sqrt{t_N} \end{bmatrix}\quad \mathbf{A}=\begin{bmatrix} A_{WP} \\ A_{WF} \\ A_{FF} \\ A_{RW} \end{bmatrix}\quad \mathbf{\Sigma}=\begin{bmatrix} s_{y,m}(t_1) \\ s_{y,m}(t_2) \\ \mathrm{M} \\ s_{y,m}(t_N) \end{bmatrix}$$

Solving this system of equations using the least squares method yields the optimal noise parameter vector.

$$\mathbf{A}=(\mathbf{M}^{\mathrm{T}}\mathbf{M})^{-1}\mathbf{M}^{\mathrm{T}}\mathbf{\Sigma} \tag{6}$$

The parameters obtained A_{WP}, A_{WF}, A_{FF} and A_{RW} are the noise parameters required to simulate atomic clock noise, which can be used for the subsequent synthesis of clock offset data.

Improved wavelet threshold function method

The core of wavelet threshold denoising is that after wavelet transformation of a signal, real information usually corresponds to wavelet coefficients with large amplitudes and small numbers, whereas noise is widely distributed in coefficients with small amplitudes. Therefore, noise suppression can be achieved by setting an appropriate threshold T and constructing a threshold function $h_T(w)$ to process each wavelet coefficient w.

The hard threshold function[4] follows a simple and straightforward rule, expressed as (7):

$$h_T^{hard}(w)=\begin{cases} w, & \text{if } |w|\geq T \\ 0, & \text{if } |w|<T \end{cases} \tag{7}$$

where w is the original wavelet coefficient; T is the threshold. This function completely preserves the coefficients with absolute values greater than or equal to the threshold T, while setting all wavelet coefficients with absolute values below the threshold to zero results in the loss of many wavelet coefficients. In addition, the function has a discontinuity at $|w|=T$, which can lead to the pseudo-Gibbs phenomenon during signal reconstruction.

To address the discontinuity issue of the hard threshold function, a soft threshold function was proposed[4].

$$h_T^{soft}(w)=\begin{cases} \mathrm{sgn}(w)(|w|-T), & \text{if } |w|\geq T \\ 0, & \text{if } |w|<T \end{cases} \tag{8}$$

The soft threshold function is continuous. For all coefficients satisfying $|w|\geq T$, there is always a constant difference of $\mathrm{sgn}(w)\times T$ between the

processed wavelet coefficient and the original coefficient w. This means that even for significant signal components with large amplitudes, unnecessary attenuation occurs, resulting in an overly smoothed post-denoising signal that loses detailed information.

To address the shortcomings of traditional hard and soft threshold functions, this paper proposes an improved threshold function based on a hyperbolic tangent smoothing transition mechanism. The expression of this function is shown in Equation (9):

$$h_T(w)=\mathrm{sgn}(w)\left(|w|-T\times\tanh\left(\frac{|w|}{d}\right)\times\tanh\left(\frac{|w|-T}{a}\right)\right) \tag{9}$$

Where $h_T(w)$ is the processed wavelet coefficient; a is the smoothing factor, which controls the transition characteristics of the function near $|w|=T$; d is the auxiliary smoothing parameter, which is set to T in this paper.

It is evident that this threshold function is continuous.

Below is an analysis of progressive behavior and deviation.

As $|w|$ approaches 0，

$$\begin{aligned}\lim_{|w|\to 0}h_T(w)&=\lim_{|w|\to 0}\mathrm{sgn}(w)\left[|w|-T\times\tanh\left(\frac{|w|}{d}\right)\times\tanh\left(\frac{|w|-T}{a}\right)\right]\\&=\lim_{|w|\to 0}\mathrm{sgn}(w)\left[|w|-T\times\frac{|w|}{T}\times\left(-\tanh\left(\frac{T}{a}\right)\right)\right]\\&=\lim_{|w|\to 0}\mathrm{sgn}(w)\left[|w|+|w|\times\tanh\left(\frac{T}{a}\right)\right]\\&=\mathrm{sgn}(w)\times|w|\times\left[1+\tanh\left(\frac{T}{a}\right)\right]\end{aligned} \tag{10}$$

the function value approaches $w\left[1+\tanh\left(\frac{T}{a}\right)\right]$, indicating that near the origin, the function value is slightly greater than the original coefficient. This facilitates the preservation of weak signal components.

At the threshold point $|w|=T$, the function value is

$$\begin{aligned}h_T(T)&=\mathrm{sgn}(w)\left(|T|-T\times\tanh\left(\frac{T}{T}\right)\times\tanh\left(\frac{T-T}{a}\right)\right)\\&=\mathrm{sgn}(w)\times[T-T\times\tanh(1)\times\tanh(0)]\\&=\mathrm{sgn}(w)\times T\end{aligned} \tag{11}$$

This indicates that no deviation exists at the threshold point.

As $|w|$ approaches ∞,

$$\begin{aligned}\lim_{|w|\to\infty}h_T(w)&=\lim_{|w|\to\infty}\left[\mathrm{sgn}(w)\left(|w|-T\times\tanh\left(\frac{|w|}{d}\right)\times\tanh\left(\frac{|w|-T}{a}\right)\right)\right]\\&=\mathrm{sgn}(w)\left(|w|-T\right)\end{aligned} \tag{12}$$

This is consistent with the asymptotic behavior of the soft threshold function.

Taking $T=1$ and $d=1$ as examples, Fig. 2 shows the hard threshold, soft threshold, and improved threshold processing methods.

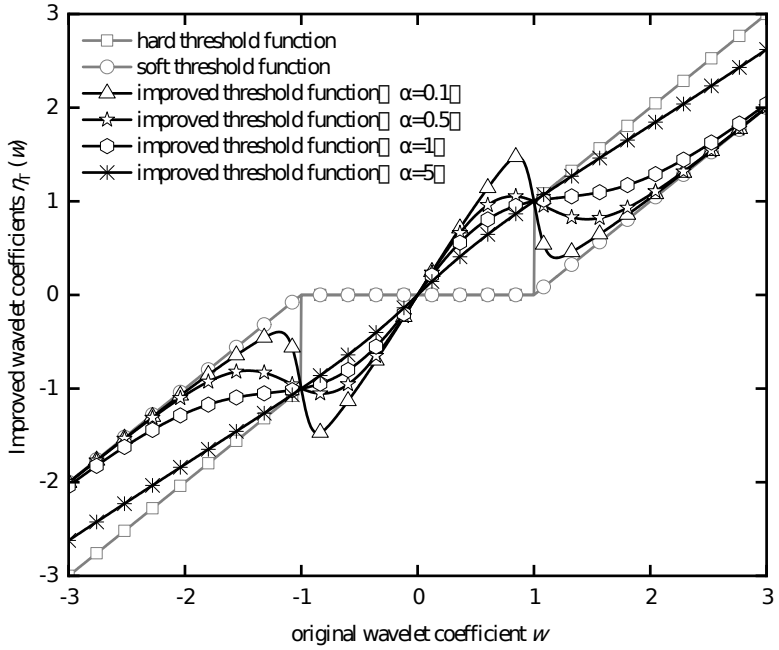

Fig. 2 Comparison of various threshold functions

As shown in Fig. 2, the hard threshold function undergoes an abrupt change at $w=\pm 1$, which verifies the discontinuity phenomenon at $w=\pm T$. The soft threshold function has a constant bias of $\mathrm{sgn}(w)\times T$ at $|w|>1$. When a is small, the improved threshold function has a certain bias in the interval $|w|>1$, but compared with the soft threshold, the bias transition near $|w|=1$ is relatively smooth. Moreover, in the interval $|w|<1$, it does not simply set the coefficients to zero but achieves a smooth transition, avoiding the abrupt truncation problem of hard and soft thresholds. As a gradually increases, the improved threshold function gradually approaches line $y=x$. When $a \to \infty$, the improved threshold function almost completely coincides with line $y=x$, at which point $h_T(w)$ approaches w, and the original wavelet coefficients w are barely processed, preserving the characteristics of the original signal.

Adaptive smoothing factor selection strategy

In the atomic clock signal denoising method based on the hyperbolic tangent smooth threshold function, the value of a directly affects the transition behavior of the threshold function between hard and soft threshold characteristics. To adapt dynamically to the nonstationary and complex noise characteristics of atomic clock signals, this paper proposes an adaptive smoothing factor selection strategy based on multifeature fusion. The core concept of this strategy is to comprehensively evaluate the current IMF component under processing based on four characteristics: noise level, kurtosis, energy dispersion, and local volatility. The evaluation results are then quantified to determine the optimal smoothing factor.

Estimation of noise levels serves as the direct basis for determining the intensity of noise reduction. The estimation method for the median absolute deviation is robust to outliers, and this method is used to estimate the standard deviation.

$$\hat{s} = \frac{Med\left(\left| w - Med(w) \right|\right)}{0.6745} \tag{13}$$

Where $Med(\ )$ is the median operator. The median absolute deviation is chosen over the sample standard deviation because atomic clock signals may exhibit frequency jumps or outliers. This leads to an overestimation of noise levels, which in turn triggers excessive noise reduction.

Kurtosis is a fourth-order statistic of a signal[16], reflecting the numerical statistical characteristics of the random variable distribution of the signal. It can be expressed as:

$$K = \frac{E(w - \bar{w})^4}{s^4} \tag{14}$$

where $\bar{w}$ and s^2 are the mean and variance of the original signal. High kurtosis values indicate that the signal contains significant physical features, requiring a small smoothing factor to preserve details.

Energy dispersion reflects the sparsity of signal energy in the wavelet domain. A larger value of energy dispersion indicates more dispersed energy and a higher proportion of noise components[17]. This indicator is defined as the complement of the ratio of the number of significant wavelet coefficients to the total number of coefficients.

$$F_{energy} = 1 - \frac{N_{sig}}{N_{total}} \tag{15}$$

Where N_{sig} is the number of significant wavelet coefficients whose absolute values are greater than the noise threshold; N_{total} is the total number of wavelet coefficients; F_{energy} is the energy dispersion.

The statistical characteristics of atomic clock signals may change over time, and relying solely on global statistics such as noise levels and kurtosis may fail to reflect local variations. Local volatility is a time-domain analysis indicator used to quantify the severity of changes in a signal between adjacent sampling points[11]. Its value is calculated as the ratio of the standard deviation of the first-order difference sequence of the signal to the standard deviation of the original sequence.

$$V_{local} = \frac{s_{Dw}}{s_w} \tag{16}$$

Where s_{Dw} is the standard deviation of the first-order difference sequence; s_w is the standard deviation of the original signal. In atomic clock signal analysis, this indicator directly reflects the short-term instability and high-frequency noise level of the signal.

Noise level serves as the basis for adjusting denoising intensity, kurtosis is used to determine whether significant physical features exist, energy dispersion reflects whether energy is concentrated, and local volatility indicates whether the signal is stable. The four characteristics above form a complementary strategy that simultaneously addresses noise levels and performance characteristics in both the time and frequency domains.

The four features above are normalized separately, yielding normalized feature values $\hat{s}$, $\hat{k}$, $\hat{F}_{energy}$ and $\hat{V}_{local}$. Calculate the composite score S using a weighted fusion strategy. $S = 0.35\hat{s} + 0.2\hat{k} + 0.25\hat{F}_{energy} + 0.2\hat{V}_{vocal}$. This paper sets the weighting ratio of noise level and energy dispersion to 60% to ensure smoothness in complex noise environments. To adapt to the sensitivity differences among different score intervals, a nonlinear mapping function is adopted to convert the comprehensive score into a smoothing factor.

$$\alpha = \begin{cases} \alpha_{min} + \dfrac{S}{0.3} \times (\alpha_{max} - \alpha_{min}) \times 0.3, & S < 0.3 \\ \alpha_{min} + \left[0.3 + (S - 0.3) \times 1.4\right] \times (\alpha_{max} - \alpha_{min}) \times 0.7, & S \geq 0.3 \end{cases} \quad (17)$$

where S is the comprehensive score obtained by weighted fusion.

Improved threshold selection strategy

In wavelet threshold denoising, the selection of the threshold directly affects the denoising effect. Traditional fixed threshold methods fail to adapt to different signal characteristics, so this paper adopts the SURE criterion as the basis for adaptive threshold selection[18].

It is assumed that the observed wavelet coefficients $w=(w_1, w_2, ..., w_N)$ are composed of a mixture of the genuine signal $s=(s_1, s_2, ..., s_N)$ and noise $n=(n_1, n_2, ..., n_N)$.

$$w = s + n, n: N(0, \sigma^2 I) \quad (18)$$

where s is the unknown genuine signal; σ^2 is the noise variance. The goal is to find an estimator $\hat{s}=h_T(w)$ that minimizes its mean squared error (MSE):

$$\mathrm{MSE} = \frac{1}{N}\sum_{i=1}^{N} E[(\hat{s}_i - s_i)^2] \quad (19)$$

Since the genuine signal is unknown, the MSE cannot be calculated directly. The SURE theorem provides a formula that relies solely on observed data w and the estimation function $h_T(w)$ to estimate the MSE in an unbiased manner. The SURE theorem states that for an estimation function $h_T(w)=(h_T(w_1), h_T(w_2), ..., h_T(w_N))$ satisfying weak differentiability, the unbiased estimator[8,11] of its risk is

$$\mathrm{SURE}(T) = -\sigma^2 + \frac{1}{N}\|h_T(w) - w\|^2 + \frac{2\sigma^2}{N}\mathrm{div}(h_T(w)) \quad (20)$$

Where $\mathrm{div}(h_T(w))$ is the divergence of the estimation function.

The traditional SURE method determines the threshold by minimizing the risk function.

$$T_{\mathrm{SURE}} = \arg\min_T \mathrm{SURE}(T) \quad (21)$$

Although the SURE criterion can provide an unbiased estimate of the MSE, it has been proven to have limitations when processing signals with complex noise. Existing studies have noted that in the context of correlated noise, the SURE criterion tends to select an excessively small threshold, leading to noise residue[19].

To avoid incomplete denoising caused by an excessively small threshold, this paper proposes a right-shifted threshold selection strategy. On the basis of the theoretically optimal threshold obtained via the SURE criterion, this strategy intentionally shifts the threshold to the right by a conservative amount to ensure the final threshold can suppress noise more sufficiently. The flow of the adaptive threshold selection algorithm is shown in

Fig. **3**.

The specific steps are as follows:

Step 1 Input wavelet coefficients and normalize

The input wavelet coefficients are normalized to unify the calculation scale.

$$w_{\mathrm{norm}} = \frac{w}{\hat{\sigma}} \quad (22)$$

Step 2 Generate candidate threshold range

Generate dense candidate thresholds within a reasonable range.

$$G = \{T_1, T_2, \ldots, T_M\}, k = 1, 2, \ldots, M \quad (23)$$

Where G is the candidate threshold range. k is the number of candidate thresholds. The threshold range selected in this paper is $[0.5\hat{s}, 4\hat{s}]$.

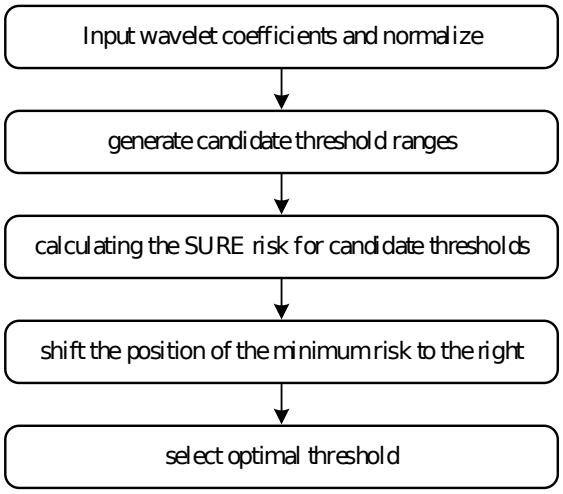

Fig. 3 Adaptive threshold selection algorithm flowchart

Step 3 Calculate the SURE risk for each candidate threshold

The SURE risk of the k-th candidate threshold is:

$$SURE(T_k) = -s^2 + \frac{1}{N}\|h_T(w) - w\|^2 + \frac{2s^2}{N}\mathrm{div}(h_T(w)) \tag{24}$$

Step 4 Shift the position of the minimum risk to the right

After the position of the minimum SURE risk is identified, the threshold corresponding to this minimum value is not adopted directly; instead, the threshold point is intentionally shifted to the right by a certain amount.

$$k_{\min} = \arg\min_k SURE(T_k) \tag{25}$$

$$k_{conservative} = \min(k_{\min} + D, M) \tag{26}$$

Where $k_{\min}$ is the position of the minimum risk, $k_{conservative}$ is the position after the rightward shift, and D is the shift amount. D can be dynamically adjusted according to the signal characteristics.

$$D = D_{base} + \left\lfloor \alpha \times f(\mathrm{SNR}) \right\rfloor \tag{27}$$

Where $f(\mathrm{SNR})$ is the SNR function. It increases the shift amount when the SNR is low and decreases the shift amount when the SNR is high.

Step 5 Select optimal threshold

The optimal threshold is determined using the offset threshold point, followed by denormalization to obtain the final optimal threshold value.

$$T_{conservative} = T_{k_{conservative}} \times \hat{s} \tag{28}$$

Where $T_{k_{conservative}}$ is the optimal threshold after shifting but before denormalization.

The flowchart of the algorithm proposed is shown in **Fig. 4**.

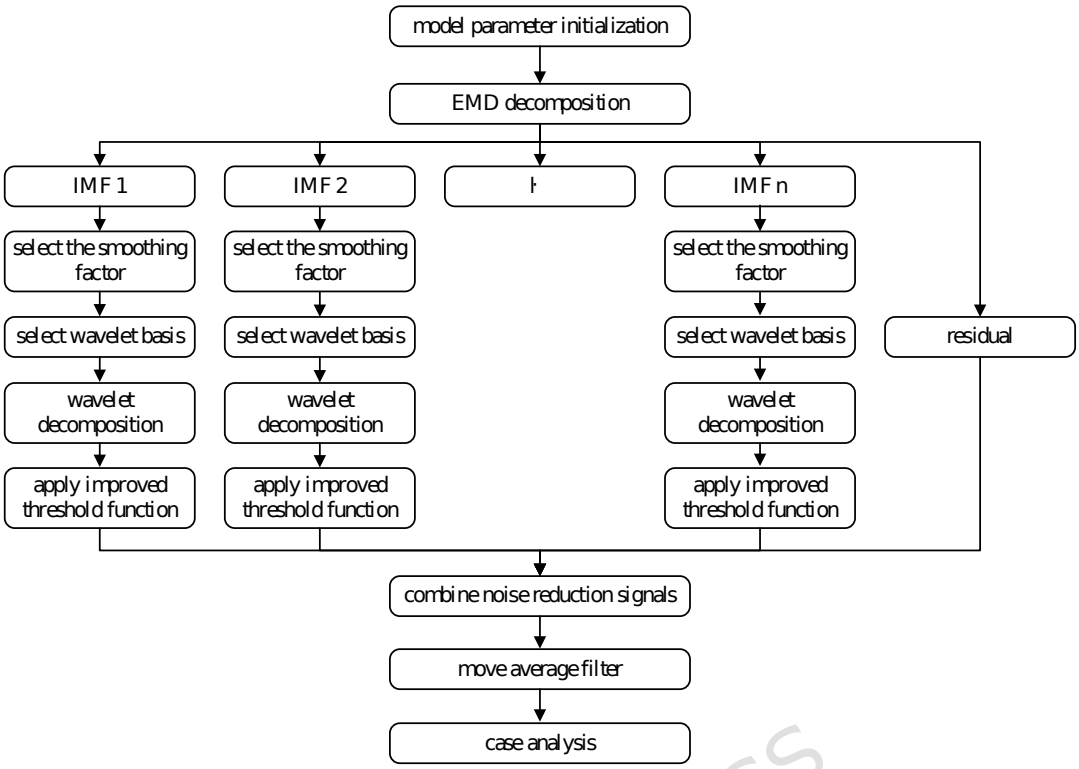

Fig. 4 Algorithm process

Case Analysis

Clock difference data analysis

Two cesium atomic clocks of different models were selected for simulation, designated as Cs1 and Cs2. Additionally, two hydrogen atomic clocks (H1 and H2) and one rubidium atomic clock (Rb1) were chosen for comparison. Utilizing their frequency stability and drift rates, the clock difference data for the atomic clocks were simulated. The performance indicators of the atomic clocks are shown in **Table. 1**.

Table. 1 Performance indicators of 5 atomic clocks

Category	Time interval/s	Cs1	Cs2	H1	H2	Rb1
frequency stability	1	5.0×10^{-12}	1.2×10^{-11}	1.5×10^{-13}	8.0×10^{-14}	2.0×10^{-11}
	10	3.5×10^{-12}	8.5×10^{-12}	2.0×10^{-14}	1.4×10^{-14}	1.0×10^{-11}
	100	8.5×10^{-13}	2.7×10^{-12}	5.0×10^{-15}	4.0×10^{-15}	3.0×10^{-12}
	1 000	2.7×10^{-13}	8.5×10^{-13}	2.0×10^{-15}	1.5×10^{-15}	2.0×10^{-12}
	10 000	8.5×10^{-14}	2.7×10^{-13}	1.5×10^{-15}	5.0×10^{-16}	2.0×10^{-12}
	100 000	2.7×10^{-14}	8.5×10^{-14}	-	-	1.0×10^{-12}
frequency drift rate	-	5.0×10^{-13}	5.0×10^{-14}	2.0×10^{-16}	3.0×10^{-16}	5.0×10^{-11}

The performance indicators of the five atomic clocks are taken as input variables and substituted into formulas (4) or (5). The least squares method

is used to solve for four noise coefficients(WPM, WFM, FFM, and RWFM). The specific solved noise coefficients are shown in **Table. 2**.

Table. 2 Noise parameters of 5 atomic clocks

Time interval/s	Cs1	Cs2	H1	H2	Rb1
WPM	9.4×10^{-12}	2.2×10^{-11}	1.3×10^{-13}	5.5×10^{-14}	1.3×10^{-11}
WFM	1.5×10^{-11}	3.5×10^{-11}	1.6×10^{-14}	2.4×10^{-14}	3.2×10^{-11}
FFM	2.9×10^{-13}	3.2×10^{-13}	1.8×10^{-15}	1.1×10^{-15}	8.8×10^{-13}
RWFM	9.9×10^{-16}	1.1×10^{-15}	5.6×10^{-18}	8.2×10^{-18}	7.3×10^{-16}

The Stable32 software is used to simulate clock offset data for five atomic clocks, collecting 5,000 data points for each clock at a 1 s interval. To validate the accuracy of the simulated data, the Allan deviation (ADEV) is calculated for each of the five simulated atomic clocks individually. The ADEV curves for the five simulated atomic clocks are shown in Fig. 5.

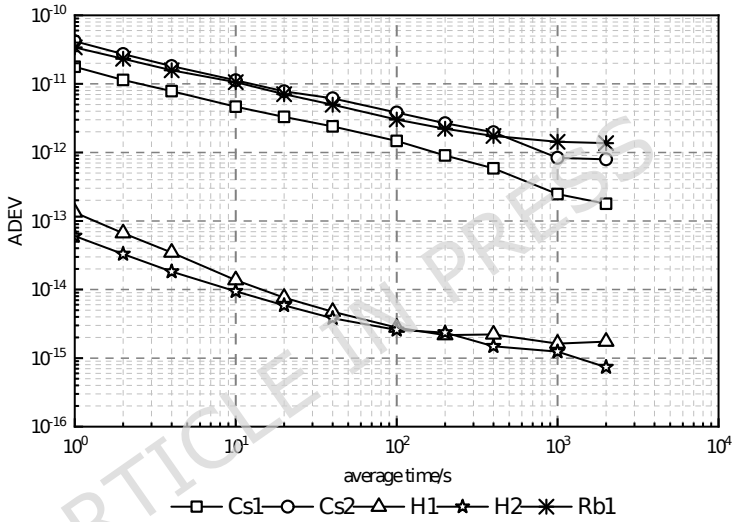

Fig. 5 Allen deviation of 5 atomic clock simulation data

As shown in Fig. 5, the ADEV curves of the two hydrogen clocks (H1, H2) almost overlap and lie at the bottom. These values are approximately two orders of magnitude lower than those of the cesium clocks, which is consistent with the theory that hydrogen masers possess excellent short-term stability due to their atomic interaction mechanism. The stability of the cesium clock Cs1 is superior to that of the cesium clock Cs2 across all average times, which aligns with the better frequency stability indicator of Cs1 in **Table. 1**. The ADEV of all the simulated clock difference data gradually decreases with increasing average time, which conforms to the characteristics of typical noise processes in atomic clocks. The stability of the simulated atomic clock data is basically consistent with that of NTSC atomic clocks, so the simulated clock difference data of the atomic clocks in this study are considered valid.

Algorithm performance analysis

For atomic clock signals, EMD can naturally separate noise mixed in different frequency bands from real signaling components on the basis of their inherent time-scale characteristics. To intuitively verify the effectiveness of EMD in atomic clock signal processing, the simulated clock

difference data of cesium clock Cs1 are taken as an example for demonstration, and its decomposition results are shown in Fig. 6.

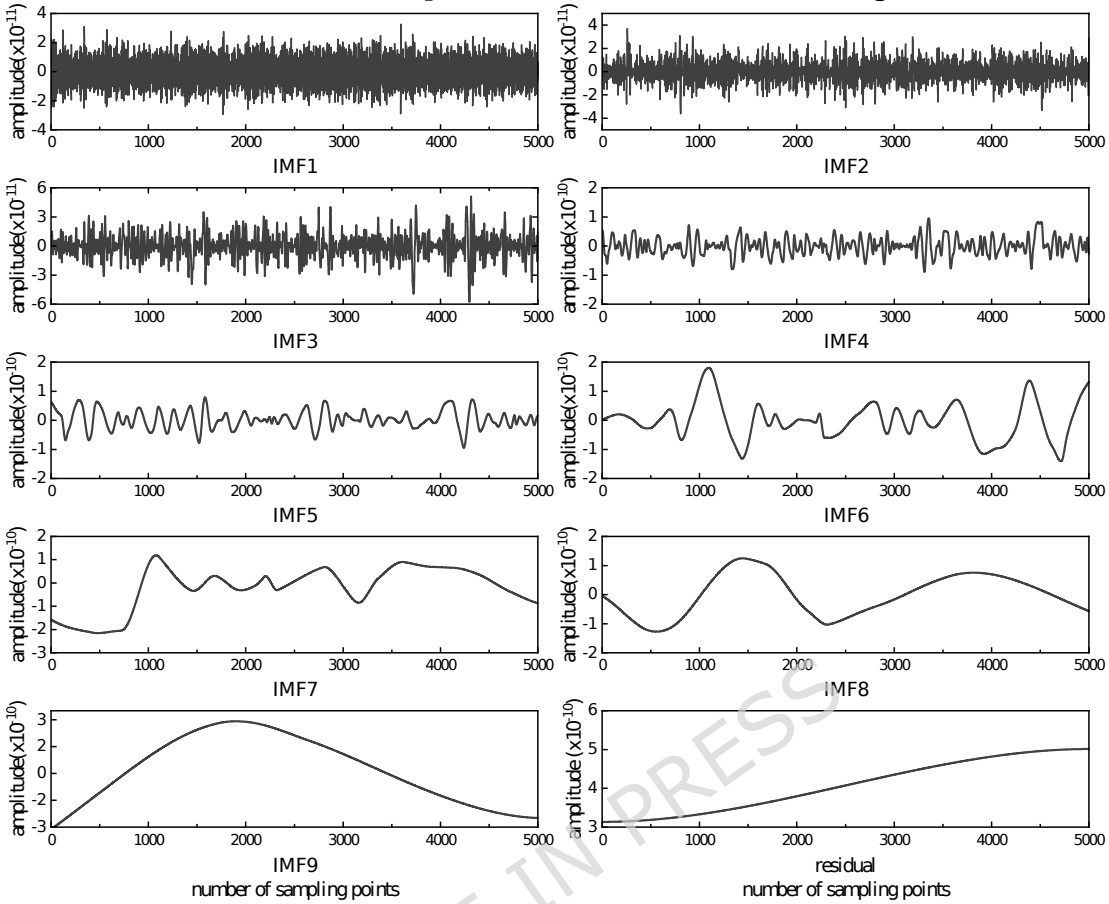

Fig. 6 Cesium clock Cs1 EMD decomposition results

For each IMF component, wavelet threshold denoising method is applied. Two metrics, SNR and RMSE, are used to assess the denoising performance of the algorithm. The SNR quantifies the power ratio between the effective components and the residual noise in the denoised clock difference signal. The higher SNR value signifies that the algorithm performs better at separating and eliminating noise energy from the observed data. The RMSE indicates the average deviation between the denoised clock difference and the original observed clock difference. The lower RMSE value suggests that the denoised signal more closely matches the original signal in terms of waveform and amplitude. The formulas for these two metrics are as follows:

$$\mathrm{SNR} = 10\lg \frac{\sum_{n=1}^{N} x^2(n)}{\sum_{n=1}^{N} [x(n) - \hat{x}(n)]^2} \tag{29}$$

$$\mathrm{RMSE} = \sqrt{\frac{1}{N}\sum_{n=1}^{N} [x(n) - \hat{x}(n)]^2} \tag{30}$$

where $x(n)$ and $\hat{x}(n)$ are the original noisy signal and the denoised reconstructed signal, $\sum_{n=1}^{N} x^2(n)$ and $\sum_{n=1}^{N} [x(n) - \hat{x}(n)]^2$ are the total power of the original signal and the total power of the noise. To verify the denoising performance of the proposed method, a rubidium atomic clock model PRS10 from the authors' laboratory, denoted rubidium clock Rb2, is selected for comparative analysis. Similarly, 5000 data points are collected with a sampling interval of 1 s. At the same time, select the method of Reference 14

for comparison. Fig. 7(a)-(f) present comparative diagrams of the clock difference data of Cs1, Cs2, H1, H2, Rb1 and Rb2 before and after denoising, where the gray curves represent the original clock difference data and the black curves represent the denoised clock difference data. **Table. 3** and **Table. 4** respectively demonstrate the denoising performance of the hard thresholding method, the soft thresholding method, and the proposed method in this paper on the clock difference data of six different types of atomic clocks.

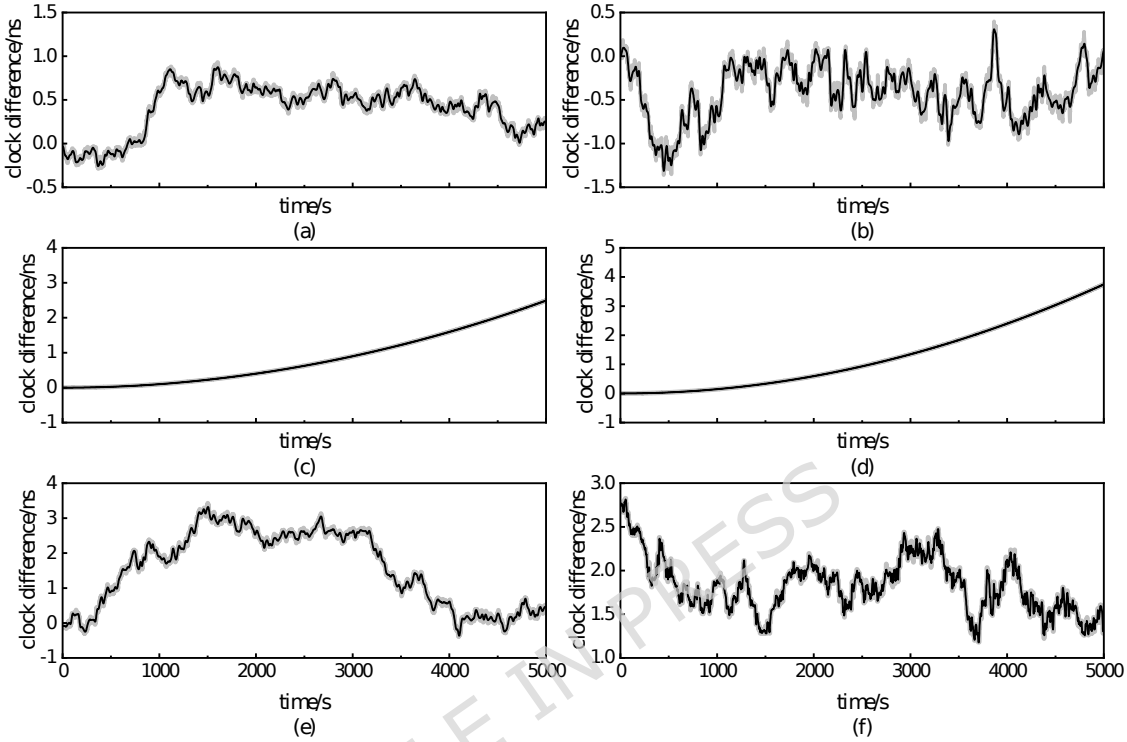

Fig. 7 Comparison of noise reduction before and after for 5 atomic clocks

Table. 3 SNRs of each threshold method under different atomic clocks(dB)

	Cesium clock		Hydrogen clock		Rubidium clock	
	Cs1	Cs2	H1	H2	Rb1 （simulated data）	Rb2 （Measured data）
hard threshold method	23.78	16.01	60.76	63.66	28.16	29.75
soft threshold method	25.63	17.77	77.86	81.71	29.99	29.88
reference 14 method	26.96	19.53	78.70	84.44	32.27	34.61
improved threshold method	28.36	20.83	81.84	86.06	33.46	37.66

Table. 4 RMSE of each threshold method under different numbers of atomic clocks($\times 10^{-11}$s)

	Cesium clock		Hydrogen clock		Rubidium clock	
	Cs1	Cs2	H1	H2	Rb1 （simulated data）	Rb2 （Measured data）
hard threshold method	3.22	8.18	0.32	0.48	7.38	6.03
soft threshold method	2.60	6.68	0.27	0.41	6.00	5.94
reference 14 method	1.99	4.94	0.22	0.39	4.83	5.02
improved threshold method	1.90	4.70	0.24	0.37	4.51	4.43

As shown in **Table. 3** and **Table. 4**, the improved threshold method proposed in this paper achieved the highest SNR and lowest RMSE values across all six atomic clocks. Specifically, compared to the soft thresholding method, the improved thresholding method enhances the SNR of cesium clocks by approximately 14%. Even for the higher-performance hydrogen clocks, an additional improvement of approximately 5% was achieved. For rubidium clock simulation data, the improved threshold method yielded an enhancement of about 11%, comparable to cesium clocks. In actual measurement data, the improved method demonstrated an increase of approximately 26%, showcasing stronger adaptability and advantages for real-world data. This result validates that the improved threshold function, by introducing a smooth transition mechanism, can more accurately distinguish between noise and signal energy. It preserves a greater number of high-amplitude wavelet coefficients reflecting genuine physical processes, thereby retaining a higher proportion of useful power in the output signal.

In terms of RMSE values, the improved threshold method achieved approximately a 28% reduction compared to the soft thresholding approach. For hydrogen clocks, while already exhibiting strong performance, the RMSE value decreased by 10%. For rubidium clocks, the improved threshold method reduced the RMSE by approximately 25% on both simulated and real-world data. This also indicates that the soft thresholding method offers limited improvement in real-world environments, while the improved method demonstrates significant advantages.

Compared to reference 14, the improved threshold method achieves performance improvements within 5% for SNR and RMSE across five sets of simulated data, and approximately 10% for measured data. Case studies demonstrate that this method effectively suppresses noise while minimizing signal distortion, thereby better preserving the original morphology and detailed features of atomic clock offset data.

Statistical Analysis

To verify that the performance improvement of the proposed method is not coincidental, we conducted a Monte Carlo analysis on simulated data. For each simulated atomic clock (Cs1, Cs2, H1, H2, Rb1), we independently generated 100 clock difference data sequences using the noise parameters, with each sequence containing 5000 data points. For each dataset, noise removal was performed using the hard thresholding method, soft thresholding method, and the improved thresholding method proposed in this paper. The SNR and RMSE were recorded for each set of experiments,

and their means and standard deviations were calculated. The results are shown in Table. 5 and Table. 6.

Table. 5 Statistical analysis of SNR performance for 20 sets of simulated data from 5 atomic clocks

	Cs1	Cs2	H1	H2	Rb1
hard threshold method	27.76 ± 4.65	24.87 ± 4.71	54.25 ± 6.86	57.44 ± 4.62	29.30 ± 5.00
hard threshold method	29.68 ± 4.63	26.69 ± 4.72	59.03 ± 6.77	59.08 ± 4.59	31.24 ± 4.95
improved threshold method	32.75 ± 4.53	29.84 ± 4.61	65.56 ± 6.71	64.13 ± 4.56	34.47 ± 4.87

Table. 6 Statistical analysis of RMSE performance for 20 sets of simulated data from 5 atomic clocks

	Cs1	Cs2	H1	H2	Rb1
hard threshold method	3.52 ±0.13	8.16 ±0.39	0.41 ±0.14	0.66 ±0.25	7.50 ±0.26
hard threshold method	2.82 ±0.10	6.62 ±0.25	0.33 ±0.12	0.61 ±0.22	5.99 ±0.16
improved threshold method	1.99 ±0.05	4.60 ±0.10	0.29 ±0.10	0.43 ±0.17	4.14 ±0.09

The statistical results in Table. 5 and Table. 6 indicate that the improved threshold method not only achieves optimal average performance in terms of SNR and RMSE but also exhibits the smallest standard deviation. This demonstrates that the proposed method possesses superior stability and repeatability, with distinct advantages for hydrogen clocks.

Time-Scale Frequency Stability Analysis

The aforementioned experiments have validated the proposed method's performance on general metrics such as SNR and RMSE, as well as its stability. To assess whether the denoised data meets practical requirements for time-frequency applications, this section analyzes time-frequency stability. Using cesium clocks to form a all-cesium clock set and hydrogen clocks to form a all-hydrogen clock set. Using the denoised data, establish time scales separately via the AT1 algorithm. The time scale established using raw data serves as a reference. The Allan deviation of the time scales is shown in Table. 7.

Table. 7 Comparison results of Allan deviation across time scales

Time interval /s	All-cesium clock set		All-hydrogen clock set	
	Denoised data	Raw data	Denoised data	Raw data
1	5.67×10^{-12}	2.12×10^{-11}	3.36×10^{-12}	1.71×10^{-11}
10	2.20×10^{-12}	7.41×10^{-12}	1.02×10^{-12}	5.65×10^{-12}
100	7.77×10^{-13}	1.45×10^{-12}	7.44×10^{-13}	2.48×10^{-12}
1000	1.65×10^{-13}	2.38×10^{-13}	1.64×10^{-13}	6.45×10^{-13}

As shown in Table. 7, for both the all-cesium clock set and the all-hydrogen clock set, the Allan deviation of the time scale established using noise-reduced data is smaller than that established using raw data. Frequency stability has significantly improved, meeting application requirements.

Conclusions

This study proposed a smooth threshold denoising method based on the hyperbolic tangent function. By introducing a smoothing factor, this function achieves a continuous transition between the characteristics of hard and soft thresholding, which not only resolves the discontinuity issue of the hard threshold function at the threshold point but also improves the constant bias defect existing in the soft threshold function. Moreover, adaptive selection of the threshold was realized by combining the SURE criterion with a rightward shift strategy, and a dynamic selection mechanism for the smoothing factor was designed, endowing the method with excellent adaptability. Case studies demonstrate that compared to conventional wavelet threshold denoising methods, the proposed approach achieves optimal performance across three distinct atomic clock signals—cesium, hydrogen, and rubidium clocks—validating its universality. Regarding noise suppression, the improved method enhances the SNR by approximately 14% and 11% for simulated cesium and rubidium clock data, respectively. For high-performance hydrogen clocks, it achieves a further 5% improvement over soft thresholding. For measured rubidium clock data, the enhancement reaches about 26%. Regarding signal fidelity, compared to soft thresholding, the improved method reduced the RMSE for cesium, hydrogen, and rubidium clocks by 28%, 10%, and 25%, respectively. The reproducibility of this method was validated through Monte Carlo analysis. Analysis of time-scale frequency stability indicates that the stability established using denoised data is significantly enhanced, meeting application requirements. The improved method proposed in this paper holds positive significance for enhancing the data quality and temporal stability of atomic clocks.

Data availability Statement

The data and software supporting the findings of this study are available upon reasonable request from the corresponding author.

References

1 Davis, J. A., Greenhall, C. A. & Stacey, P. W. A Kalman filter clock algorithm for use in the presence of flicker frequency modulation noise. *Metrologia* **42**, 1-10, (2005).

2 Song, H., Dong, S., Wang, X., Zhang, Y. & Wang, Y. An improved Kalman filter time scale algorithm for atomic clock noise variation. *Acta Phys. Sin.* **69**, 212-220, (2020).

3 Ke, X., Li, X., Liu, Z. & Deng, F. Stability analysis of a time scale algorithm. *Chinese Astronomy and Astrophysics* **26**, 245-253, (2002).

4 Klionskiy, D., Kupriyanov, M. & Kaplun, D. Signal denoising based on empirical mode decomposition. *Journal of Vibroengineering* **19**, 5560-5570, (2017).

5 Li, X., Liao, K., He, G. & Zhao, J. Research on Improved Wavelet Threshold Denoising Method for Non-Contact Force and Magnetic Signals. *Electronics* **12**, 1244, (2023).

6 Li, Z., Yao, X., Zhang, C., Qian, Y. & Zhang, Y. Vibration Signal Noise-Reduction Method of Slewing Bearings Based on the Hybrid Reinforcement Chameleon Swarm Algorithm, Variate Mode Decomposition, and Wavelet Threshold (HRCSA-VMD-WT) Integrated Model. *Sensors* **24**, 3344, (2024).

7 Donoho, D. L. De-noising by soft-thresholding. *IEEE Transactions on Information Theory* **41**, 613-627, (1995).
8 Qu, T., Dai, T. & Wang, S. Adaptive Wavelet Thresholding Denoising method Based on SURE Estimation. *ACTA ELECTRONICA SINICA* **30**, 266-268, (2002).
9 Meng, J., Pan, J. & Zhang, H. Denoising by Multiscale Product Coefficient Semi-soft Thresholding. *journal of Electronics & Information Technology* **29**, 1649-1652, (2007).
10 Tao, K. & Zhu, J. A Hybrid Indicator for Determining the Best Decomposition Scale of Wavelet Denoising. *Acta Geodaetica et Cartographica Sinica* **41**, 749-755, (2012).
11 Wu, G., Wang, C., Bao, J., Chen, Y. & Hu, Y. A Wavelet Threshold De-noising Algorithm Based on Adaptive Threshold Function. *Journal of Electronics & Information Technology* **36**, 1340-1347, (2014).
12 Liu, X., Bian, S., Zhai, G. & Li, S. The improved wavelet filtering algorithm based on Stein's unbiased risk estimation. *Science of Surveyimg and Mapping* **49**, 158-166, (2024).
13 Jiang, M. *et al.* Fusion of hydrogen and cesium time scale based on Vondark-Cepek filter. *Chinese Journal of Scientific Instrument* **40**, 158-166, (2019).
14 Galleani, L., Sacerdote, L., Tavella, P. & Zucca, C. A mathematical model for the atomic clock error. *Metrologia* **40**, 257-264, (2003).
15 Zhao, S., Dong, S., Bai, S., Wang, Y. & Qu, L. Research on the frequency steering algorithm of time-keeping frequency standard and primary frequency standard. *Chinese Journal of Scientific Instrument* **41**, 67-75, (2020).
16 Xiao, D., Ding, J., Li, X. & Huang, L. Gear Fault Diagnosis Based on Kurtosis Criterion VMD and SOM Neural Network. *Applied Sciences* **9**, 5424, (2019).
17 Donoho, D. L. & Johnstone, I. M. Ideal Spatial Adaptation by Wavelet Shrinkage. *Biometrika* **81**, 425-455, (1994).
18 Donoho, D. L. & Johnstone, I. M. Adapting to Unknown Smoothness via Wavelet Shrinkage. *Journal of the American Statistical Association* **90**, 1200-1224, (1995).
19 Johnstone, I. M. & Silverman, B. W. Wavelet Threshold Estimators for Data with Correlated Noise. *Journal of the Royal Statistical Society. Series B (Methodological)* **59**, 319-351, (1997).

Author contributions

X.N. analyzed the data, and wrote the manuscript. D.H. and Z.W. contributed to data collection and analysis. X.N. and L.W. planned and designed the experiments conducted the experiments. Q.L. reviewed and revised the manuscript. All authors reviewed and approved the final manuscript.

Funding
This work was supported by the National Social Science Foundation(2022-SKJJ-B-050).

Competing interests
The authors declare no competing interests.

Additional information
Correspondence and requests for materials should be addressed to D.H.